The FASEB Journal

FASEB
Federation of American Societies for Experimental Biology

RESEARCH ARTICLE OPEN ACCESS

Mouse NR2E3^{R296Q} Mutation Disrupts Photoreceptor Developmental Paradigm and Leads to Early-Onset Progressive Retinal Degeneration by Suppressing RXRG Signaling

Jiacheng Jin | Shuai Wang | Yinjiu Huang | Shanglun Xie

School of Life Sciences, Anhui Provincial Key Laboratory of Tumor Evolution and Intelligent Diagnosis and Treatment, Bengbu Medical University, Bengbu, Anhui, P.R. China

Correspondence: Shanglun Xie (shanglunxie@bbmu.edu.cn) | Yinjiu Huang (yinjiuhuang1973@163.com)

Received: 4 December 2024 | **Revised:** 2 March 2025 | **Accepted:** 27 March 2025

Funding: The present study was supported by the National Natural Science Foundation of China (Grant 32200479), the Natural Science Foundation of Anhui Province (Grant 2108085QC99), the talent project of Anhui Educational Committee (Grant 2024AH030041), and the Natural Science Foundation of Bengbu Medical University (Grant 2024bypy014).

Keywords: CRISPR-Cas9 | ESCS | NR2E3^{R296Q} mutation | photoreceptor development | retinal degeneration | RXRG signaling

ABSTRACT

The NR2E3^{R311Q} mutation can lead to retinitis pigmentosa, enhanced S-cone syndrome (ESCS), Goldmann–Favre syndrome, and clumped pigmentary retinal degeneration. The relationship between this mutation and various recessive inherited retinal degenerative disorders is unclear and complicates clinical diagnosis and treatment. In this study, we generated a mouse strain carrying the NR2E3^{R296Q} mutation using CRISPR/Cas9 technology to simulate the NR2E3^{R311Q} mutation in humans and investigate the influence of this missense mutation on the photoreceptor developmental profile and retinal maintenance. Retinal architecture and lamination were normal in NR2E3^{R296Q} mice. Whorls and rosettes were not observed in the outer nuclear layer (ONL). Rod cell quantity developed normally, whereas a small amount of Rhodopsin was incorrectly located in the ONL. Blue cones were excessively produced at the dorsal retina, whereas green cone development was normal. Colocalization of Rhodopsin and Arrestin occurred in the retinas of NR2E3^{R296Q} mice. Heterozygous NR2E3$^{+/R296Q}$ mice showed no evident abnormalities in retinal structure or photoreceptor development. Retinas of NR2E3^{R296Q} mice underwent progressive degeneration starting in the early postnatal stage, which manifested as reduced ONL thickness and outer segment fragmentation. The dorsal retina, where redundant blue cones are generated, degenerated in a more advanced manner. At the molecular level, NR2E3 bound directly to the *RXRG* promoter, whereas the NR2E3 R296Q mutation significantly impaired binding, resulting in significantly decreased *RXRG* mRNA and protein expressions. In summary, we developed a novel mouse model exhibiting an ESCS-like phenotype, thus providing a novel NR2E3-RXRG signaling pathway for modulating photoreceptor development and retinal maintenance.

Abbreviations: Chip-Seq, chromatin immunoprecipitation sequencing; CPRD, clumped pigmentary retinal degeneration; CRX, cone-rod homeobox protein; DBD, DNA-binding domain; ESCS, enhanced S-cone syndrome; GFS, Goldmann–Favre syndrome; LBD, ligand-binding domain; NR2E3, nuclear receptor subfamily 2 group E member 3; NRL, neural retina leucine; ONL, outer nuclear layer; PCR, polymerase chain reaction; RP, retinitis pigmentosa; TEM, transmission electron microscopy; WT, wild-type.

Jiacheng Jin and Shuai Wang contributed equally to this work.

1 | Introduction

Vision plays a crucial role in learning, working, and other daily activities. Vision loss decreases productivity, affects psychology, and reduces quality of life [1]. Humans have a duplex retina assembled from two types of photoreceptors: rods and cones [2]. Rods are sensitive to dim light and function at night and in dark conditions, whereas cones are sensitive to bright light during the day and are responsible for color recognition. Dysfunction in rod or cone photoreceptors can lead to retinal degenerative diseases, such as retinitis pigmentosa (RP) [3] and age-related macular degeneration [4]. Mammalian rods and cones are derived from common retinal progenitor cells, with their differentiation tightly regulated by a group of evolutionarily conserved transcription factors, including cone-rod homeobox protein (CRX) [5], neural retina leucine zipper (NRL) [6], and nuclear receptor subfamily 2 group E member 3 (NR2E3) [7].

NR2E3, also known as the photoreceptor-specific nuclear receptor, is abundantly expressed in retinal tissues and plays a pivotal role in modulating photoreceptor fate specification and retinal maintenance [8]. Mutations in human *NR2E3* lead to RP, enhanced S-cone syndrome (ESCS), Goldmann–Favre syndrome (GFS), and clumped pigmentary retinal degeneration (CPRD) [9]. Over 80 pathogenic variants of the human *NR2E3* gene have been reported [10], most of which are located in the DNA-binding domain (DBD), which mediates DNA recognition, and in the ligand-binding domain (LBD), which binds hydrophobic ligands and regulates transcriptional activity of target genes as well as dimer formation [9]. Except for a defined p.Gly56Arg mutation in the DBD region causing autosomal dominant RP [11, 12], clear genotype–phenotype correlations among recessively inherited diseases have not been established. For instance, the p.Arg311Gln mutation ($NR2E3^{R311Q}$) in the LBD region, which has the highest incidence, can lead to recessive RP, ESCS, GFS, and CPRD [10, 13]. The mechanisms through which the $NR2E3^{R311Q}$ mutation affects photoreceptor development and how this consistent variation causes different degenerative outcomes have not been investigated.

Animal models are valuable tools for studying the biological functions of defined proteins. The rd7 mouse, which carries a naturally occurring *NR2E3* nonsense mutation, exhibits an ESCS-like phenotype [14, 15]. Using this model, researchers have reported that NR2E3, in synergy with CRX and NRL, performs a dual regulatory function by enhancing rod gene expression and suppressing cone gene transcription in rod precursors [16]. NR2E3 suppresses cone development by inhibiting the proliferation of retinal progenitors [17]. In zebrafish, *NR2E3* elimination generates RP-like features, according to the phenotype in which rod differentiation is prevented; cones develop normally during the juvenile period but gradually degenerate after 1 month of age [18]. Ablation of different domains of mouse NR2E3 results in RP-like and ESCS-like phenotypes [19]. Although the functions of NR2E3 have been extensively studied, major issues remain to be addressed. For example, mutations in the rd7 mouse and $NR2E3^{-/-}$ zebrafish are nonsense, whereas pathogenic mutations in humans are often missense. Different mutation types can lead to divergent functions of NR2E3 proteins; therefore, the pathogenesis of retinal degeneration may differ between animals with *NR2E3* nonsense mutations and humans with $NR2E3^{R311Q}$ variations. Therefore, a unique animal model is required to determine the retinal phenotype (RP-like or ESCS-like) in a mammalian organism carrying the parallel mutation and to elucidate the underlying mechanisms through which this mutation disrupts the photoreceptor developmental profile and impairs retinal maintenance.

Similar to the $NR2E3^{R311Q}$ mutation in humans, we constructed a mouse strain carrying the p.Arg296Gln mutation ($NR2E3^{R296Q}$) using CRISPR-Cas9 technology. We observed that the homozygous $NR2E3^{R296Q}$ mouse exhibits an ESCS-like phenotype. In addition, the $NR2E3^{R296Q}$ mutation disrupts photoreceptor development and results in retinal degeneration by impairing RXRG signaling. Here, we report our detailed findings based on the $NR2E3^{R296Q}$ mouse model.

2 | Materials and Methods

2.1 | Animals and Ethical Approval

$NR2E3^{R296Q}$ mice were created using CRISPR/Cas9 (GemPharmatech). The mice were maintained in a 12-h light/dark cycle with *ad libitum* access to food and water. The animals used in this study were the offspring of $NR2E3^{+/R296Q}$ heterozygous parent mice. Approvals for all the procedures conducted in this study were given by the Experimental Animal Ethics Committee of Bengbu Medical University (approval number: 2022032) prior to their initiation.

2.2 | Mouse Genotype Identification

Mouse tails were treated with 100 μL of 0.2% NaOH, followed by lysis on a shaker (MQT-60R, Servicebio) at 55°C and 100 rpm for 10 h. For final lysis, 10 μL of Tris–HCl (pH 8.0) was added to the solution. Polymerase chain reaction (PCR) was performed using 2 μL of the lysis solution and the 2× Rapid Tap Master Mix in a T100 Thermal Cycler (621BR21585, Bio-Rad). PCR products were visualized using agarose gel electrophoresis and sequenced at Sangon Biotech (Shanghai, China). The primers used for genotype identification are listed in Table S1.

2.3 | Western Blot Analysis

The retinal tissues were isolated from the eyes of the mice with various genotypes and lysed in 200 μL of RIPA buffer (P0013B, Beyotime) supplemented with 2 μL of phenylmethanesulfonyl fluoride (PMSF) (ST506, Beyotime). To each sample, 50 μL of 5× SDS-PAGE loading buffer (P0015, Beyotime) was added, followed by incubation at 100°C for 5 min (min). Subsequently, the samples were loaded onto 10% SDS-PAGE gels (PG112, Epizyme Biomedical Technology), where proteins were separated via electrophoresis and transferred onto polyvinylidene fluoride membranes (FFP28, Beyotime). These membranes were blocked with specialized reagents (P0023B, Beyotime) and incubated with the primary antibodies overnight at 4°C, followed by a 2-h incubation with the secondary antibodies at room temperature. Images were captured using the ChemiDoc

XRS+ system (Universal Hood II, Bio-Rad). Protein images from the ChemiDoc XRS+ system were analyzed in triplicates using ImageJ (v2.14.0). Table S2 lists the primary and secondary antibodies used in this study.

2.4 | Quantitative PCR

The retinal tissues were placed in 1 mL of TRIzol reagent and were homogenized using a homogenizer (KZ-III-F, Servicebio). Following the homogenization, 0.2 mL of trichloromethane was added to the samples. The mixture was centrifuged at 4°C for 15 min, and the resulting supernatant was aspirated before the addition of 0.5 mL of isopropanol. The mixture was then centrifuged at 4°C for 10 min, washed twice with 75% ethanol, and centrifuged again at 4°C for 5 min. The RNA quality was assessed using a microspectrophotometer (NanoDrop one, Thermo Fisher). The complementary DNA was synthesized in accordance with the instructions provided by the manufacturer (R323-01, Vazyme). Quantitative PCR (qPCR) was performed using 2 × RealStar Fast SYBR qPCR Mix (A304-05, GenStar) on a LightCycler Green instrument (055815916001, Roche), following the instruction manual for specific steps, with β-actin as the reference gene. Table S1 lists the primer sequences used for qPCR.

2.5 | Hematoxylin–Eosin Staining and Immunofluorescence

Mice were euthanized by cervical dislocation, and their eyes were collected and fixed overnight at 4°C in 4% paraformaldehyde (P0099, Beyotime). The eyes were dehydrated in a 30% sucrose solution until it sank to the bottom of the tube. The eyes were embedded, and the frozen sections measuring 10 μm were prepared using a microtome cryostat (CM1950, Leica).

For HE staining, the cryosections were fixed in 4% paraformaldehyde for 20 min at room temperature. The sections were washed thrice with double-steamed water and stained with hematoxylin (C0105S, Beyotime) for 4 min at room temperature. Following the three additional washes, the sections underwent a 40-s differentiation in an acid-alcohol solution (C0161S, Beyotime). After an additional wash, eosin (C0105S, Beyotime) staining was performed on the sections for 5 min. The sections were subsequently dehydrated in ethanol solutions of varying concentrations (70%, 80%, 90%, and 100%) before being mounted using a nail polish. Images were captured using an upright optical microscope (Nikon Eclipse E100, Nikon).

For immunofluorescence (IF) experiments, the retinal sections were permeabilized in a photodynamic therapy (PDT) solution (PBS containing 1% DMSO and 0.1% TritonX-100) for 10 min and blocked with a 10% goat serum (C0265, Beyotime) in PBDT (PDT containing 1% BSA) for 1 h. The sections were subsequently incubated overnight at 4°C with the primary antibody. The following day, the sections were washed thrice with PDT and incubated with the secondary antibodies at 37°C for 2 h. The nuclei were stained with 2-(4-amidinophenyl)-6-indolecarbamidine dihydrochloride (DAPI). The sections were mounted with an antifade mounting medium (P0126, Beyotime), and the images were captured using a scanner (Pannoramic MIDI, 3DHISTECH). The primary and secondary antibodies used for IF tests are listed in Table S2.

2.6 | Chip-Seq and Chip-qPCR

Adeno-associated viruses carrying flag-tagged wild-type (WT) NR2E3 and NR2E3^{R296Q} mutant expression vectors were designed by Obio Technology (Shanghai, Chian) and administered into the subretinal space. For crosslinking, the retinal tissues were treated with 27 μL of 37% formaldehyde for 10 min at 22°C. Chromatin immunoprecipitation sequencing (Chip-Seq) was performed using GeneBook (Wuhan, China) with an anti-flag antibody. The Chromatin Immunoprecipitation Kit (JKR23002A, Genecreate) and the DNA Purification Kit (D0033, Beyotime) were used to acquire the chromatin DNA that was immunoprecipitated via flag antibody. Chip-qPCR was performed to analyze the binding interactions of NR2E3 and NR2E3^{R296Q} with the RXRG promoter. The primer sequences are listed in Table S1.

2.7 | Transmission Electron Microscopy

The eyes of the mouse were fixed in an electron microscopy fixative (G1102, Servicebio) at room temperature for 2 h, dissected into appropriately sized sections, and fixed overnight at 4°C. The samples were washed thrice with 0.1 M PBS (pH 7.4) for 15 min each, and subsequently fixed in 1% osmium tetroxide for 2 h at room temperature. The eyes were dehydrated through sequential incubations for 20 min in increasing concentrations of ethanol: 30%, 50%, 70%, 80%, 95%, and 100%. Subsequently, the eyes were incubated in acetone for 15 min and treated with 50% (3 h), 66% (overnight), and 100% (6 h) epoxy resin (mixed with acetone). Thereafter, the samples were heated at 37°C overnight and subsequently at 60°C for 48 h; the embedded eyes were sliced into ultrathin sections (80 nm) using an ultramicrotome (LeicaUC7, Leica). These sections were stained with 2% uranyl acetate in a saturated alcohol solution for 8 min and washed thrice with 70% alcohol. Further, the sections were washed thrice with ultrapure water and stained using 2.6% lead citrate for 8 min. After the three additional washes with ultrapure water and subsequent drying, images were captured using transmission electron microscopy (TEM) (HT7800, HITACHI).

2.8 | RNA Sequencing

The integrity of total RNA samples from WT and NR2E3^{R296Q} mice was quantified using a Bioanalyzer 2100 system (TapeStation Analysis 5.1). The RNA samples with OD260/280 between 1.8 and 2.0, RIN ≥ 6.5, 28S/18S ≥ 1.0, and total RNA > 2 μg were selected for RNA sequencing (RNA-seq). The library was prepared by purifying messenger RNA (mRNA) from total RNA using poly(T)-oligo-attached magnetic beads, followed by fragmentation, amplification, and subsequent purification. After establishing the library quality control using Qubit and real-time PCR, different libraries were pooled

based on the effective concentration and the targeted data amount. Thereafter, they were subjected to Illumina sequencing. High-quality clean data were obtained by removing the adapter sequences, poly-N reads, and low-quality reads from the raw data.

Gene expression levels were quantified using featureCounts software (v1.5.0-p3), and differential gene expression analysis was performed using the DESeq2 package in R (v1.20.0). After using the Benjamini–Hochberg method to control the error discovery rate, differentially expressed genes were identified with a p value threshold of ≤ 0.05. Furthermore, Gene Ontology (GO) and KEGG pathway analyses were conducted to determine the enrichment of the differentially expressed genes.

2.9 | Statistical Analysis

Data from all experiments are presented as mean ± SD and analyzed for significant differences between the means of two independent groups using an unpaired two-tailed t-test. A p value <0.05 was considered statistically significant ($^{*}p<0.05$; $^{**}p<0.01$; $^{***}p<0.001$). Statistical analyses were performed using the GraphPad Prism software (v9.4.0). The quality control was ensured by performing the experiments in triplicates.

3 | Results

3.1 | Generation of NR2E3^{R296Q} Mutant Mice

To develop a mammalian model with the equivalent NR2E3^{R311Q} mutation observed in humans, we first aligned the NR2E3 peptide sequences across various organisms. The arginine at position 311 in humans is highly conserved among mammals (Figure 1A), indicating its important and conserved functions in mammals. Consequently, mammals with corresponding variations were appropriate for simulating the human NR2E3^{R311Q} mutation. The guanine and adenine at positions 887 and 888 on exon 6 of mouse *NR2E3* were mutated to adenine and guanine, respectively, using CRISPR-Cas9 technology, resulting in a substitution of arginine with glutamine at position 296 (Figure 1B). After crossing and screening for several generations, we obtained the wild-type (WT), heterozygous (NR2E3$^{+/R296Q}$), and homozygous (NR2E3^{R296Q}) mice (Figure 1C).

The mRNA expression of *NR2E3* was not changed in NR2E3$^{+/R296Q}$ and NR2E3^{R296Q} mice (Figure 1D), whereas the protein levels were increased with no significant difference (Figure 1E,F), indicating that this missense mutation did not alter the transcriptional and translational activity of the *NR2E3* gene.

3.2 | Retinal Morphology Developed Normally in NR2E3^{R296Q} Mice

To determine if the NR2E3^{R296Q} mutation leads to developmental defects in mouse retinas, we conducted a histological analysis using hematoxylin and eosin (HE) staining on postnatal day 14 (P14). Compared to WT mice, no apparent abnormalities were observed in NR2E3$^{+/R296Q}$ retinas (Figure 2A,B). Morphology and lamination were standard in NR2E3^{R296Q} retinas, although the thickness of the outer nuclear layer (ONL) was decreased, with no statistical significance (Figure 2A,B). Unlike the rd7 and NR2E3 functional domain-ablated mouse strains, which exhibit ONL whorls and rosettes starting at P12 [15, 19, 20], the NR2E3^{R296Q} retina was flat and had no similar anomalies (Figure 2A).

3.3 | Rhodopsin Mislocalization and Overproduction of Blue Cones Are Observed in the Retinas of NR2E3^{R296Q} Mice

Nonsense mutations in rd7 mice and zebrafish consistently disrupt the developmental patterns of photoreceptors [16–18]. To assess whether the NR2E3^{R296Q} mutation leads to developmental anomalies in mouse photoreceptors, immunofluorescence experiments were performed on P14 using antibodies specific to anti-Rhodopsin, OPN1SW, and OPN1MW to mark rods, blue cone photoreceptors, and green cone photoreceptors, respectively. We determined that the Rhodopsin content of NR2E3$^{+/R296Q}$ and NR2E3^{R296Q} retinas was comparable to that in WT mice; however, a small amount of Rhodopsin was retained in ONL (Figure 3A), indicating that heterozygous and homozygous NR2E3^{R296Q} mutations do not alter the production of normal numbers of rods but lead to the incorrect localization of Rhodopsin. Notably, this was not observed in nonsense mutant rd7 mice and *NR2E3*$^{-/-}$ zebrafish [17, 18]. Generation of blue cones was markedly increased in the dorsal retinas of NR2E3^{R296Q} mice but was not altered in NR2E3$^{+/R296Q}$ mice (Figure 3B,H). Development of green cones was not affected in heterozygous and homozygous NR2E3^{R296Q} mice (Figure 3C).

To confirm these phenotypes, we immunolabeled the opsin proteins after 2.5 months. The mislocalization of Rhodopsin and significantly increased amounts of blue cones in the dorsal retina were again observed in NR2E3^{R296Q} mice (Figure 3D–F,I). The expression of another cone marker, Arrestin, was prominently upregulated (Figure 3G,J). Furthermore, the expression of these opsin proteins was quantified using western blotting, and the results were consistent with the IF data (Figure 3K–O). Collectively, these findings indicate that the NR2E3^{R296Q} mutation causes a small amount of Rhodopsin to mislocalize as well as an increase in the number of blue cones in the dorsal retina.

3.4 | Colocalization of Rhodopsin and Arrestin Was Observed in NR2E3^{R296Q} Mice

NR2E3 nonsense mutations in rd7 mice generate "hybrid" photoreceptors that simultaneously express rod and cone genes [21]. To determine whether similar phenotypes are observed in NR2E3^{R296Q} missense mutant mice, retinal sections were immunolabeled with anti-Rhodopsin (rod-specific) and anti-Arrestin (cone-specific) antibodies after 2.5 months. We observed that these two proteins were labeled together in a portion of photoreceptors in NR2E3^{R296Q} mice (Figure 4), indicating the presence of intermediate photoreceptors similar to those observed in rd7 mice.

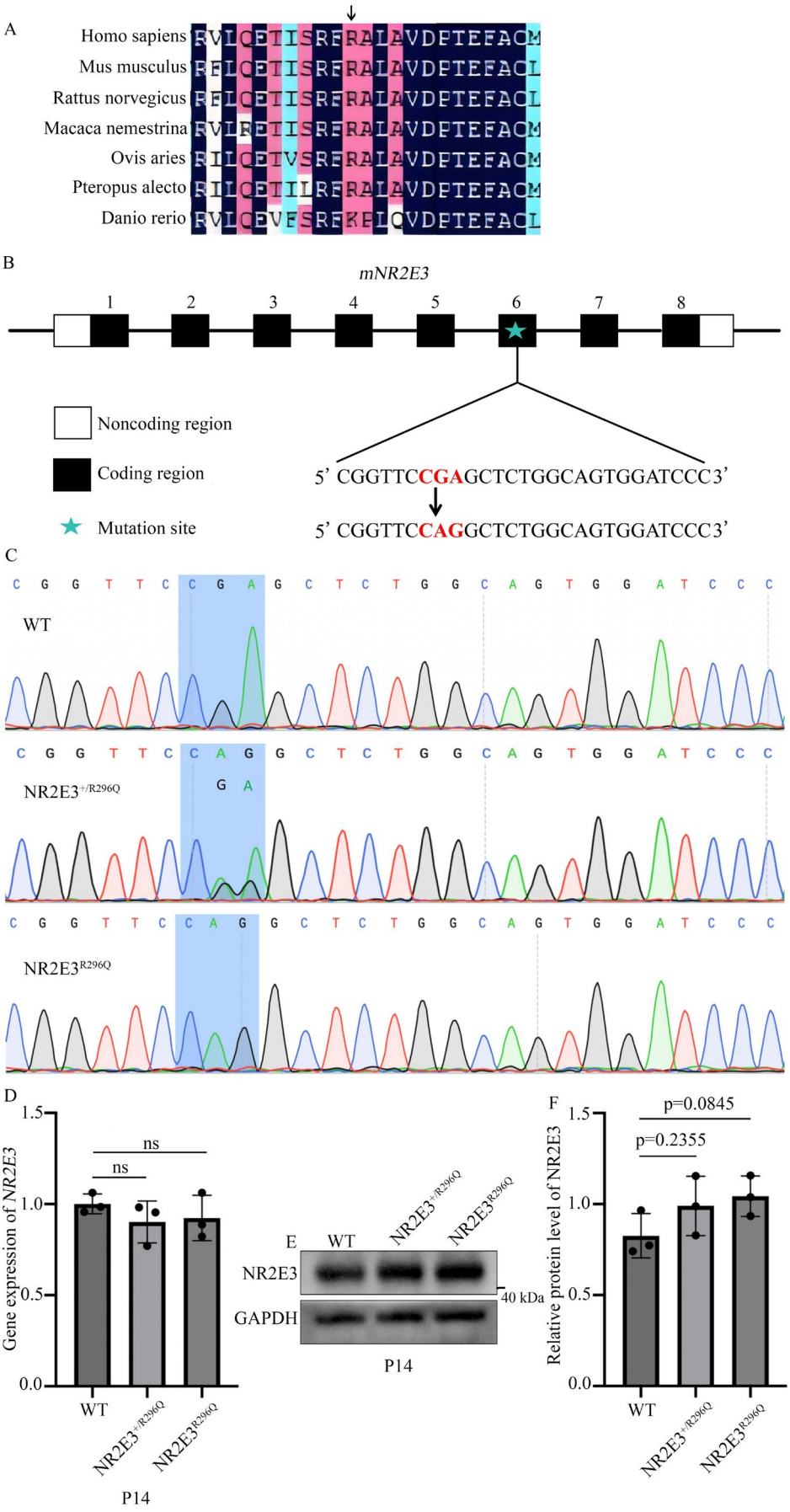

FIGURE 1 | Legend on next page.

FIGURE 1 | Construction and identification of mouse NR2E3^{R296Q} missense mutation. (A) Conservation analysis of arginine at position 311 in human NR2E3 (mammals) and zebrafish. The black arrow indicates the arginine at position 311 in human NR2E3 and position 296 in mouse NR2E3. (B) Gene structure of mouse *NR2E3* and the target site used to generate NR2E3^{R296Q} missense mutation. The bases marked in red represent the codon encoding arginine at position 296 in wild-type (WT) NR2E3 and Gln in mutant NR2E3. (C) DNA sequence validation of the NR2E3^{R296Q} mutation. WT, wild-type; NR2E3$^{+/R296Q}$, heterozygous; NR2E3^{R296Q}, homozygous; the base marked with shadow represents the target mutated sequence. (D) mRNA levels of *NR2E3* in retinal tissue from the specified genotype measured using qPCR at P14. Data are shown as mean ± SD (SD) ($n = 3$). β-Actin served as the endogenous control. "ns" denotes no significant difference. (E, F) Protein levels of NR2E3 in retinal tissue from the specified genotype measured using the western blot (WB) test at P14. Glyceraldehyde-3-Phosphate Dehydrogenase (GAPDH) was used as the loading control. Data are shown as mean ± SD (SD) ($n = 3$).

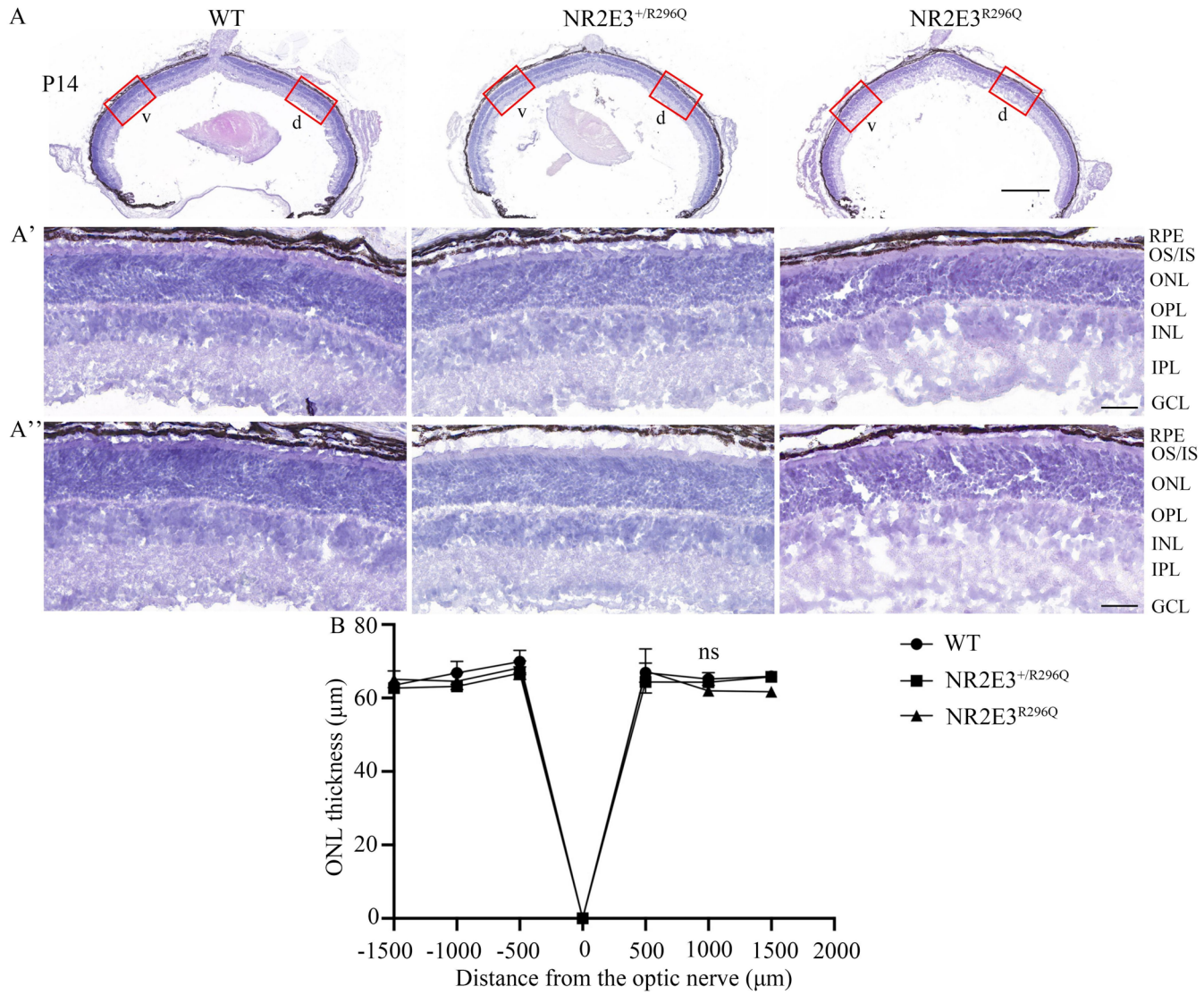

FIGURE 2 | Retinal histological analysis in NR2E3$^{+/R296Q}$ and NR2E3^{R296Q} mice. (A) HE staining performed to assess retinal architecture and lamination in mice with the specified genotypes at P14. Scale bar: 0.5 mm. (A′) and (A″) show magnified images in the dorsal and ventral retina in (A), respectively. d, dorsal retina; v, ventral retina. Scale bar: 0.05 mm. (B) Statistical analysis of ONL thickness at different positions from the optic nerve. Data are presented as mean ± SD (SD) ($n = 3$). "ns" indicates no significant difference.

3.5 | NR2E3^{R296Q} Mice Exhibit Early-Onset and Progressive Retinal Degeneration

Humans with NR2E3^{R311Q} mutations have a degenerated retina [22]. In addition to developmental dysplasia in NR2E3 nonsense mutant rd7 mice and zebrafish, retinal degeneration has been observed in these animals in adulthood [18, 20]. To assess whether the NR2E3^{R296Q} mutation causes retinal degeneration in mice, HE staining was conducted after 2.5 and 8 months. Compared to the contemporary WT control, NR2E3^{R296Q} retinas exhibited significant degeneration, which manifested as a decrease in ONL thickness and whole retinal thickness. NR2E3^{R296Q} retinal degeneration was more notable in the dorsal region, approximately 1000 μm from the optic nerve, a position

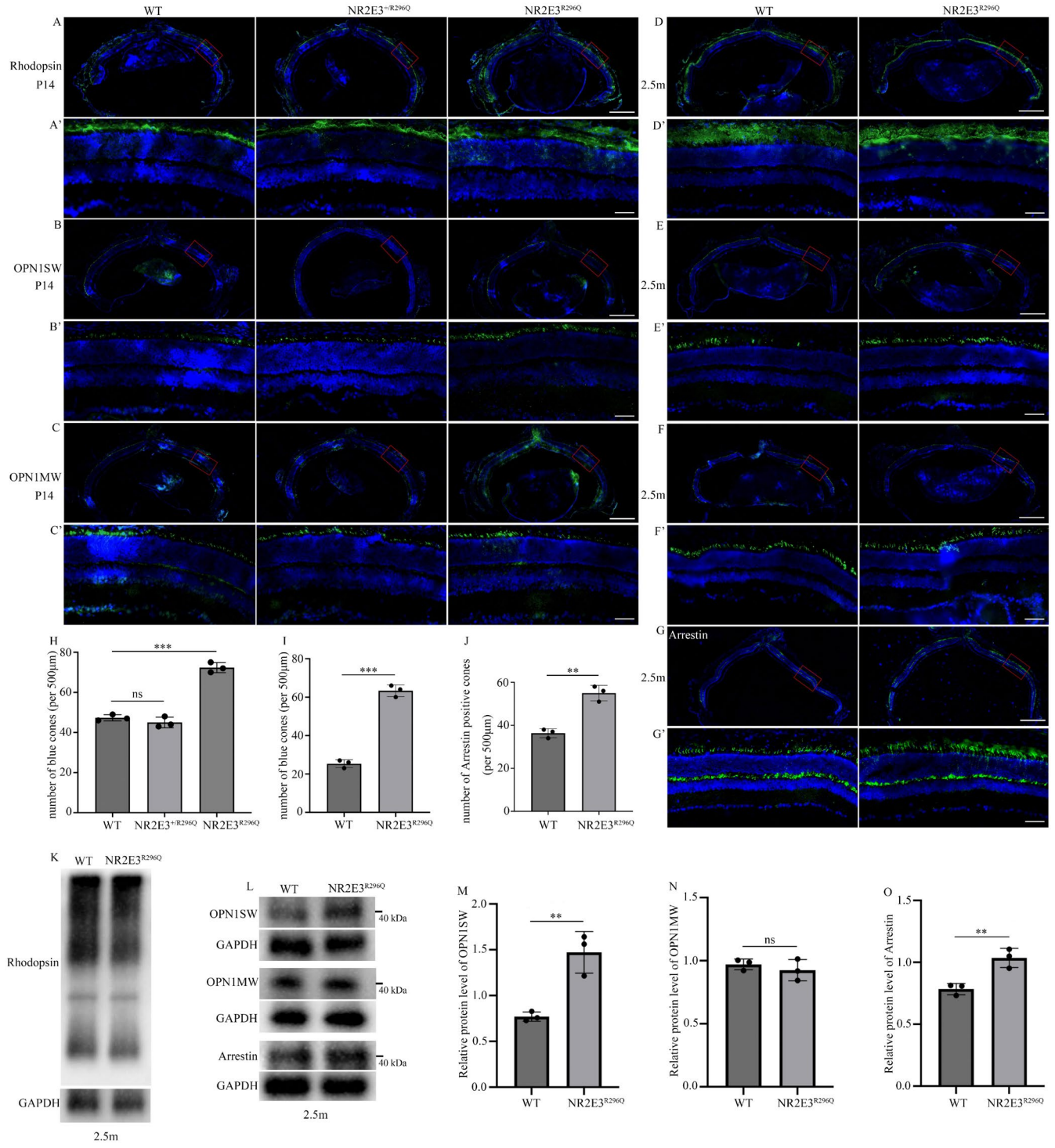

FIGURE 3 | Blue cones were redundantly generated in the dorsal retina in NR2E3^{R296Q} mice. Retinal cryosections from mice of the specified genotypes were immunostained with anti-Rhodopsin (A), anti-OPN1SW (B), and anti-OPN1MW (C) antibodies at P14. Scale bars: 0.5 mm. (A'), (B′), and (C′) represent the magnified figures in (A), (B), and (C), respectively. Scale bars: 0.05 mm. Retinal sections from wild-type (WT) and NR2E3^{R296Q} mice were immunostained with anti-Rhodopsin (D), anti-OPN1SW (E), anti-OPN1MW (F), and anti-Arrestin (G) antibodies at 2.5 m. Scale bars: 0.5 mm. (D′), (E′), (F′), and (G′) show the amplified images from (D), (E), (F), and (G), respectively. Scale bars: 0.05 mm. Statistical analysis of blue cones in the boxed dorsal retina at P14 (H) and 2.5 m (I). "ns" indicates no significant difference. ***$p < 0.001$. Data are presented as mean ± SD (SD) ($n = 3$). (J) Statistical analysis of Arrestin-positive cone photoreceptors in the boxed dorsal retina at 2.5 m. **$p < 0.01$. Data are presented as mean ± SD (SD) ($n = 3$). (K, L) Protein levels of Rhodopsin, OPN1SW, OPN1MW and Arrestin were detected in WT and NR2E3^{R296Q} mice at 2.5 m using western blotting (WB), and glyceraldehyde-3-phosphate dehydrogenase (GAPDH) was used as the endogenous control. (M–O) Statistical data of OPN1SW, OPN1MW and Arrestin protein levels. "ns" indicates no significant difference. **$p < 0.01$. Data are presented as mean ± SD (SD) ($n = 3$).

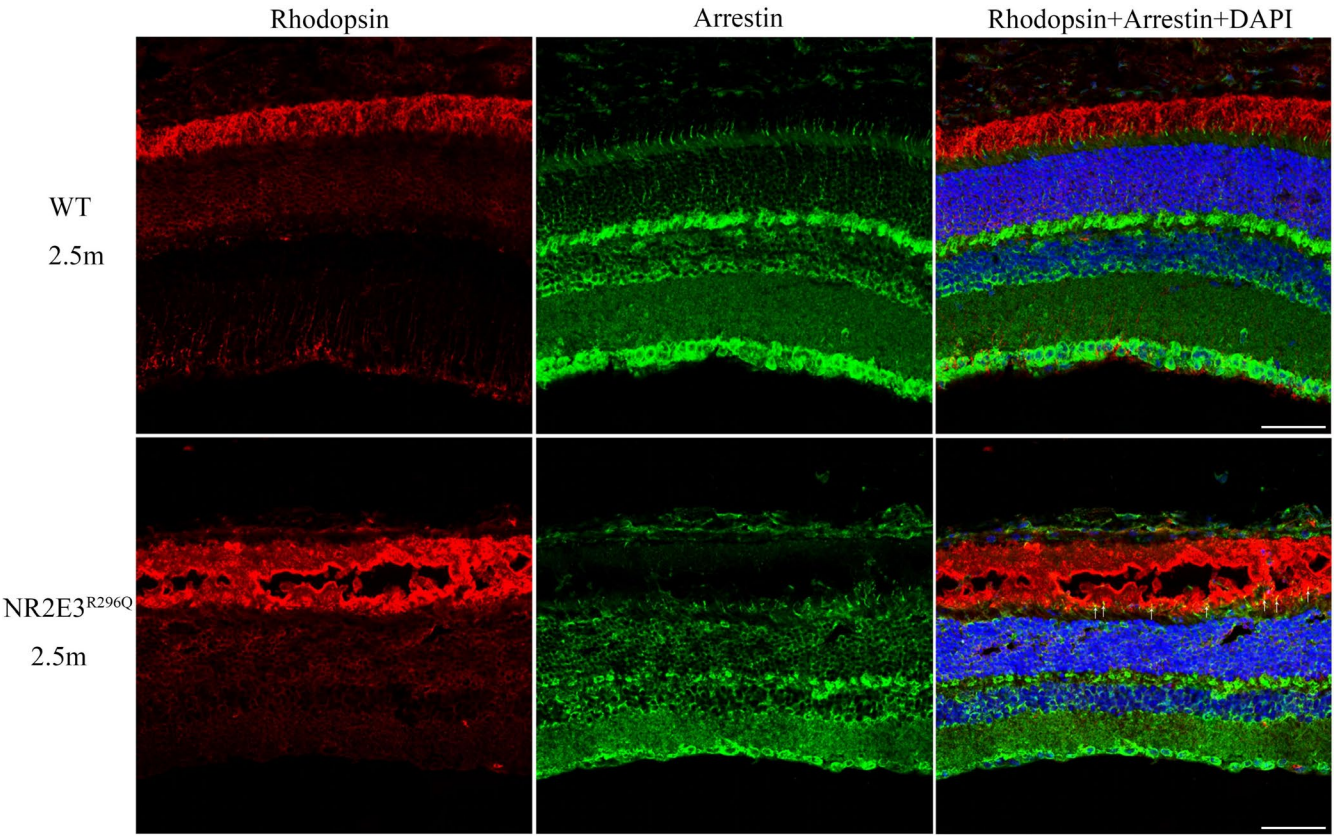

FIGURE 4 | Rhodopsin and Arrestin were simultaneously expressed in the retinas of NR2E3^{R296Q} mice. Retinal slices were double-immunolabeled with anti-Rhodopsin and anti-Arrestin antibodies at 2.5 m (white arrows indicating double-labeled photoreceptors). Scale bars: 0.5 mm.

that enhanced blue cone photoreceptor density (Figure 5A–D). After 2.5 months, degeneration primarily affected the dorsal retina (Figure 5A,C); however, after 8 months, degeneration had spread throughout the retina (Figure 5B,D). Transmission electron microscopy (TEM) experiments were performed to observe the ultrastructure of the photoreceptor outer segment and nucleus on P14. Compared to WT control, the distribution of euchromatin and heterochromatin in the nuclei of NR2E3^{R296Q} mice showed no significant abnormalities (Figure 5E); however, the membranous discs in the NR2E3^{R296Q} retinas were disorganized and fragmented (Figure 5F). Combined with the slight thinning of the ONL in NR2E3^{R296Q} mice on P14 (Figure 2A), our data indicate that the NR2E3^{R296Q} mutation leads to early-onset and progressive retinal degeneration, which is similar to the clinical characteristics of ESCS. In addition, NR2E3$^{+/R296Q}$ mice revealed no developmental anomalies in the retinal architecture and photoreceptor composition, which is consistent with the recessive genetic model of ESCS.

3.6 | NR2E3^{R296Q} Mutation Disrupts the RXRG Signaling Pathway

We identified the molecular mechanisms through which the NR2E3^{R296Q} mutation results in excessive blue cone photoreceptors. Considering that NR2E3 functions as a transcription factor modulating the transcriptional activity of target genes, we used chromatin immunoprecipitation sequencing (ChIP-seq) to identify target genes differentially bound by the wild-type NR2E3 and NR2E3^{R296Q} proteins. Owing to the lack of NR2E3 antibodies for CHIP analysis, we constructed vectors expressing flag-tagged wild-type and NR2E3^{R296Q} mutant proteins, encapsulated in adeno-associated virus (AAV), and injected into the subretinal space to infect retinal tissue. When the wild-type NR2E3 was immunoprecipitated, abundant binding peaks at the transcription start site (TSS) (I) and promoter region (II, III) of *RXRG* were observed; however, this binding was significantly reduced when the NR2E3^{R296Q} mutant protein was immunoprecipitated (Figure 6A), indicating that although the wild-type NR2E3 binds to the TSS and promoter region, the NR2E3^{R296Q} mutation disrupts this binding. Homer motif analysis further identified several binding motifs (Figure 6B), including CCTCTGC(A)A (−2033 bp) and GTTCGTG(A)T (−1890 bp) located at the promoter region.

RXRG encodes a nuclear receptor protein that belongs to the retinoid X receptor (RXR) family and modulates photoreceptor development in chickens and zebrafish [23, 24]. RXRG is co-expressed with NR2E3 in the mouse retina [25], and a nonsense mutation in RXRG results in the overproduction of blue cones in the dorsal retina without influencing green cone development [26]. These phenotypes are consistent with the developmental patterns of blue and green cone photoreceptors in our NR2E3^{R296Q} mouse model. In addition, mRNA and protein levels of *RXRG* were significantly downregulated in NR2E3^{R296Q} retinas (Figure 6C–E). ChIP and ChIP-quantitative polymerase chain reaction (qPCR) were performed to confirm the binding of NR2E3 to the *RXRG* promoter. Consistent with the ChIP-seq results, wild-type NR2E3 bound directly to the *RXRG* promoter (−1999 to −1869 bp), whereas the NR2E3^{R296Q} mutant did not

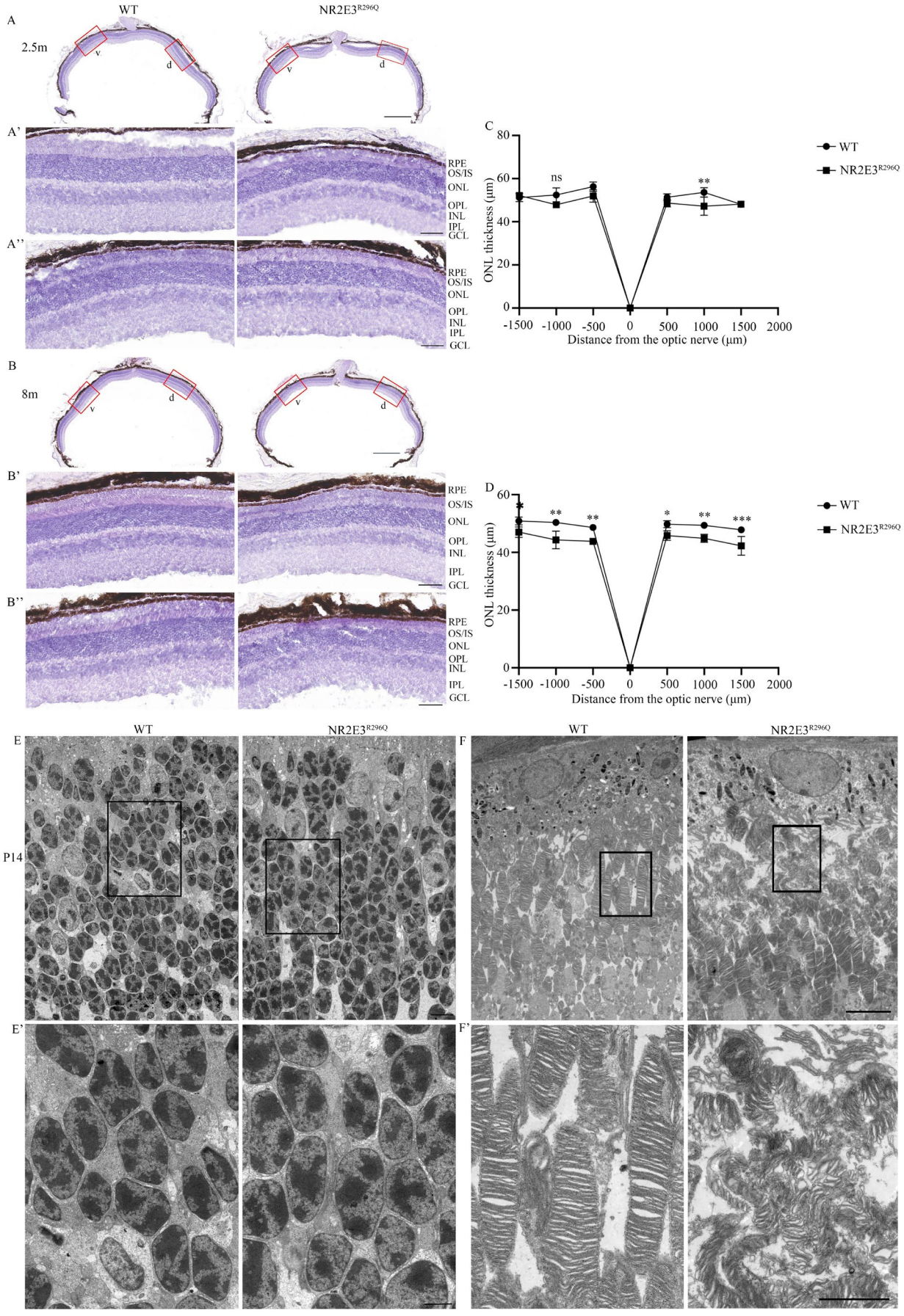

FIGURE 5 | Legend on next page.

FIGURE 5 | Retina gradually degenerated in NR2E3^{R296Q} mice. Retinal histological analysis was conducted using HE staining at 2.5 m (A) and 8 m (B). Scale bars: 0.5 mm. (A′) and (A″) represent the enlarged images in dorsal and ventral retinas in (A), respectively. (B′) and (B″) represent magnified views of the dorsal and ventral retinas in (B), respectively. d, dorsal retina; v, ventral retina. Scale bars: 0.05 mm. Statistical data of ONL thickness at varying positions from the optic nerve were performed at 2.5 m (C) and 8 m (D). (C) and (D) are presented as mean ± SD ($n = 3$). "ns" indicates no significant difference. *$p < 0.05$, **$p < 0.01$, ***$p < 0.001$. Ultrastructural analysis of the nucleus (E) and membrane disc (F) was performed at P14 using TEM. Scale bars: 5 μm. (E′) and (F′) show the magnified image of (E) and (F), respectively. Scale bars: 2 μm.

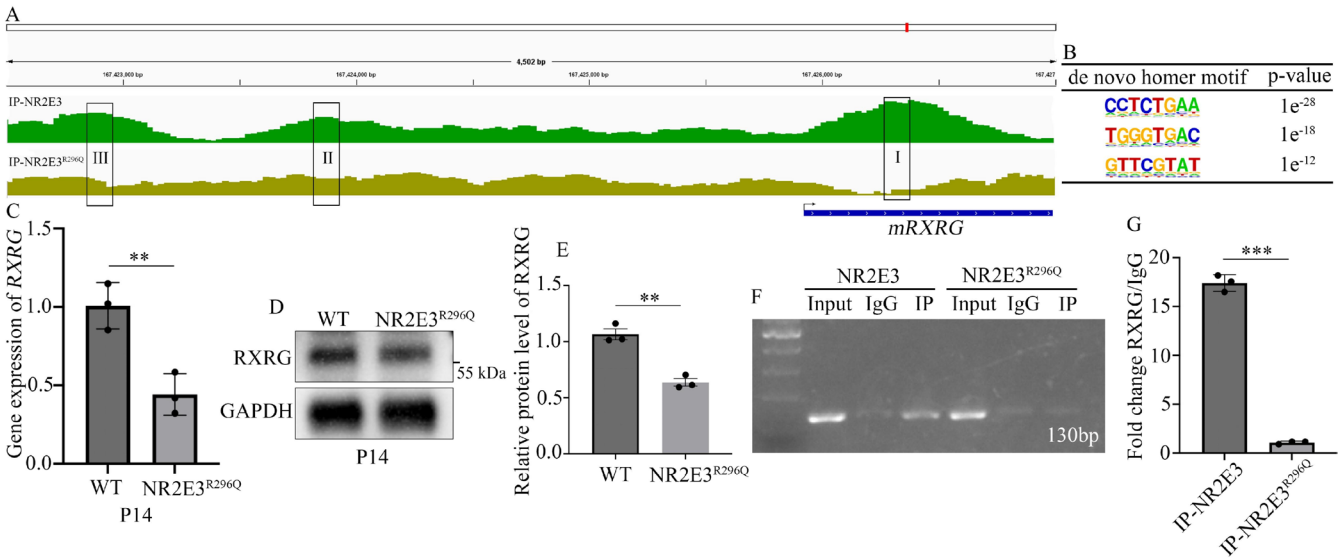

FIGURE 6 | NR2E3^{R296Q} Mutation suppresses *RXRG* expression. (A) Chip-seq analysis reveals binding peaks enriched at the transcription start site (TSS) (I) and promoter region (II, III) of *RXRG* immunoprecipitated from wild-type and NR2E3^{R296Q} proteins. (B) Predicted binding sites of NR2E3 on the *RXRG* promoter were identified using a *de novo* Homer motif analysis algorithm. (C) *RXRG* mRNA expression was examined in NR2E3^{R296Q} mice at P14 using qPCR. Data are presented as mean ± SD (SD) ($n = 3$), with β-Actin serving as the endogenous control. **$p < 0.01$. (D) RXRG protein levels were detected in NR2E3^{R296Q} mice at P14 using western blotting (WB), and glyceraldehyde-3-phosphate dehydrogenase (GAPDH) was used as the endogenous control. (E) Statistical data of RXRG protein levels in (D). **$p < 0.01$. Data are presented as mean ± SD (SD) ($n = 3$). (F) ChIP and (G) ChIP-qPCR confirmed the direct binding of NR2E3 to the *RXRG* promoter region (II), while the NR2E3^{R296Q} mutation impaired this binding. ***$p < 0.001$. Data are presented as mean ± SD (SD) ($n = 3$).

(Figure 6F,G). Collectively, these results indicate that RXRG is a direct downstream target of NR2E3 in the regulation of photoreceptor development in the mouse retina. The NR2E3^{R296Q} mutation suppresses *RXRG* expression, thereby altering the photoreceptor developmental profile.

3.7 | Transcriptome Dynamics Analysis in NR2E3^{R296Q} Retinas

We investigated the transcriptome dynamics in NR2E3^{R296Q} mouse retinas using RNA sequencing (RNA-seq) on P14. A total of 178 (fold change [FC] ≥ 2, adjusted p value ≤ 0.05, fragments per kilobase of transcript per million mapped reads [FPKM] > 0) differentially expressed genes (DEGs) were detected (Figure 7A). The RNA levels of *rhodopsin, gnat1, pde6a, pde6b* (rod-specific), and *opn1mw* (green cone-specific) were unaffected (Figure 7A) and were consistent with normal rod and green cone development in the NR2E3^{R296Q} retina (Figure 3A,C,D,F) and their expression patterns in rd7 mice [16]. Interestingly, RNA levels of *opn1sw* and *arrestin* were not significantly altered (Figure 7A), indicating that potential mechanisms may regulate the expression of these two genes at the protein level. CRX and NRL were expressed at normal levels (Figure 7A), which is consistent with the reported opinion that these two factors act upstream of NR2E3 to mediate photoreceptor differentiation [27]. The RNA level of NR2E3 itself was comparable between WT and NR2E3^{R296Q} mice (Figure 7A) and was consistent with the qPCR results (Figure 1D).

Functional clustering analysis revealed that several biological processes and molecular functions were affected by the NR2E3^{R296Q} mutation, including cell fate commitment and intracellular receptor signal transduction (Figure 7B,C). Microfilament motor and cytoskeletal motor activities were reduced (Figure 7B), which may account for the mislocalized Rhodopsin (Figure 3A,D) and disorganized outer segment in the retinas of NR2E3^{R296Q} mice (Figure 5F).

4 | Discussion

The NR2E3^{R311Q} mutation results in RP, ESCS, GFS, and CPRD [9]. The unclear association between this mutation and diverse recessive disorders poses challenges for functional research and treatment exploration. In the present study, we developed a new mouse strain carrying the NR2E3^{R296Q} mutation

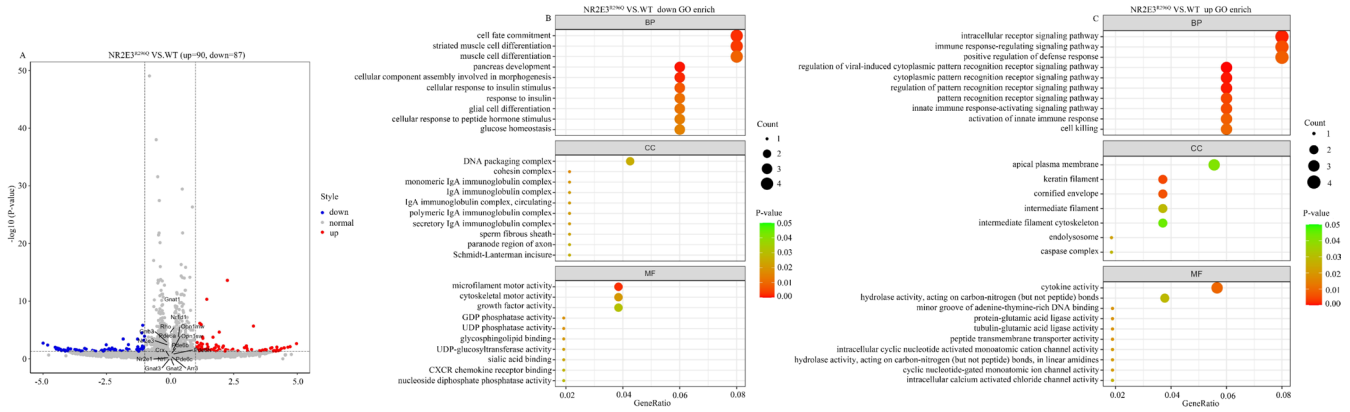

FIGURE 7 | Transcriptome dynamics analysis in NR2E3^{R296Q} mice using RNA-seq method. (A) A volcano plot showing differentially expressed genes (90 upregulated and 87 downregulated) between WT and NR2E3^{R296Q} retinas at P14. The red, blue, and gray points represent upregulated, downregulated, and non-significantly differentially expressed genes, respectively. Gene ontology (GO) enrichment analysis of enriched downregulated (B) and upregulated (C) genes, highlighting enriched biological processes (BP), cellular components (CC), and molecular functions (MF) in NR2E3^{R296Q} mice.

to simulate the NR2E3^{R311Q} mutation in humans. We observed that NR2E3^{R296Q} mice exhibited an ESCS-like phenotype characterized by redundant blue cone photoreceptor generation and progressive retinal degeneration. In addition, the NR2E3^{R296Q} protein disrupted photoreceptor development by targeting RXRG signaling, which differs from the nonsense mutation that disrupts classical CRX-NRL-NR2E3 signaling [27].

In most retinal degenerative diseases, the function of photoreceptors, including rods and all types of cones, is attenuated, whereas in ESCS, the ability of the blue cone is enhanced based on an increase in the number of these cells [28]. Several research groups have studied the reasons for the increased blue cone in ESCS. Using rd7 mice, researchers have shown that the supernumerary blue cones can be generated from transdifferentiation of plastic rod precursors [16, 21], and/or result from the prolonged proliferation of retinal progenitors [17]. In mammals, a portion of rods was recruited from blue cones in the normal developmental program [29]. In the present study, NR2E3^{R296Q} mice possess excessive blue cones and intermediate hybrid photoreceptors. Collectively, these results support the opinion that rod precursors transform to blue cones once normal NR2E3 is lost.

Determining the cellular localization of NR2E3 is crucial for elucidating the cellular origin of excess blue cones; however, this has not yet been thoroughly studied. Chen et al. reported that NR2E3 is expressed only in postmitotic rod precursors [16], whereas Haider et al. showed that NR2E3 is expressed in mitotic retinal progenitors and developing and mature cones [17, 25]. Although we attempted to determine the cellular localization of NR2E3, we were unable to obtain a working antibody that recognizes NR2E3 in the IF test. Other technologies, such as single-cell sequencing, may be required to accurately identify the detailed cellular expression of *NR2E3*.

An interesting phenomenon is that the role of NR2E3 in mediating rod development appears to differ between humans and mice. Mutations in human NR2E3, including nonsense and missense variations, cause night blindness owing to early loss of rod function [7]. In contrast, rod development remained normal in the rd7 mouse and our NR2E3^{R296Q} model (although a small amount of Rhodopsin was incorrectly located). The electrophysiological function of the rod in rd7 mice was normal before 6 months [30]. Although NR2E3 enhances the transcriptional activity of rhodopsin in vitro [31], the mRNA and protein expression of rhodopsin and other rod-specific phototransduction genes in vivo were normal [16, 17, 21].

NR2E3 strongly controls rod development in zebrafish, where its absence leads to a complete lack of rods in *NR2E3*$^{-/-}$ zebrafish retinas [18]. The pivotal factor controlling rod generation in mice is NRL, as rods do not exist in *NRL*$^{-/-}$ mice [32]. A comprehensive analysis showed that the function of NR2E3 in mediating rod development is not conserved in both humans and mice.

The heterogeneity of pathogenic genes and pathological features hinders the expansion of clinical treatment for RP [33]; however, NR2E3 represents a promising target to develop a broad-spectrum and gene-independent method to treat retinal degenerative disease based on the following reports: (1) AAV-mediated *NR2E3* delivery promotes retinal homeostasis and attenuates and ameliorates retinal degeneration in multiple animal models (including rd7 mouse) [34]; (2) *NR2E3* knockout shifts rods toward a hybrid rod-cone-like phenotype, thereby conferring strong neuroprotective effects on rod and cone photoreceptors in degenerating retinas [35]. AAV-mediated *NR2E3* gene therapy (OCU400, Ocugen) was approved to conduct clinical trials by the FDA. In the present study, we investigated the effect of a single amino acid change (R296Q) on NR2E3 activity, showing the role of the NR2E3-RXRG axis in photoreceptor development and maintenance. Our data expand the current understanding of protein function and may contribute to the development of targeted therapies.

NR2E nuclear receptors (including NR2E3) are the most closely related members to RXR subgroups [36]. NR2E3 and RXRG are co-expressed in the mouse retina, and functional changes in NR2E3 and RXRG result in a similar phenotype, that is, the overproduction of blue cones in the dorsal retina [26]. Pathogenic mutations in the DBD abolish the recognition of NR2E3 by the target DNA sequences [37]. In this study, we observed that the

NR2E3^{R296Q} mutation, located in the LBD region, compromised its binding to the *RXRG* promoter. The LBD is known to mediate homologous and heterologous dimerization [38]. NR2E3^{R311Q} mutation impairs NR2E3 homodimerization and heterodimerization with PPARG and TRβ2, two nuclear receptor proteins that play important roles in photoreceptor development [38]. Therefore, the NR2E3^{R296Q} mutant protein may disrupt homo- or heterodimer formation, thus altering the conformation of the protein complex and changing the binding preference for DNA sequences.

Collectively, coupled with decreased *RXRG* expression in the NR2E3^{R296Q} retina, our results indicate that RXRG is involved in the NR2E3 signaling axis regulation of photoreceptor development. However, to the best of our knowledge, the role of RXRG in retinal maintenance has not been investigated, making its expression profile at the late-life stage in NR2E3^{R296Q} mice worth analyzing. Interestingly, both NR2E3 and RXRG may have anti-inflammatory effects in degenerating retinas [39, 40], and novel anti-inflammatory strategies targeting NR2E3-RXRG signaling may be designed from it.

Author Contributions

Jiacheng Jin, Yinjiu Huang, and Shanglun Xie conceived and designed the research. Jiacheng Jin and Shuai Wang performed the research and acquired the data. Jiacheng Jin and Shuai Wang analyzed and interpreted the data. Jiacheng Jin and Shanglun Xie wrote the manuscript. Shuai Wang and Yinjiu Huang revised the manuscript. Yinjiu Huang and Shanglun Xie funded the research.

Conflicts of Interest

The authors declare no conflicts of interest.

Data Availability Statement

The data that support the findings of this study are available on request from the corresponding author.

References

1. F. Liu, Y. Y. Qin, Y. W. Huang, et al., "Rod Genesis Driven by Mafba in an Nrl Knockout Zebrafish Model With Altered Photoreceptor Composition and Progressive Retinal Degeneration," *PLoS Genetics* 18 (2022): e1009841.

2. T. D. Lamb, "Evolution of Phototransduction, Vertebrate Photoreceptors and Retina," *Progress in Retinal and Eye Research* 36 (2013): 52–119.

3. D. T. Hartong, E. L. Berson, and T. P. Dryja, "Retinitis Pigmentosa," *Lancet* 368 (2006): 1795–1809.

4. L. S. Lim, P. Mitchell, J. M. Seddon, F. G. Holz, and T. Y. Wong, "Age-Related Macular Degeneration," *Lancet* 379 (2012): 1728–1738.

5. T. Furukawa, E. M. Morrow, and C. L. Cepko, "Crx, a Novel Otx-Like Homeobox Gene, Shows Photoreceptor-Specific Expression and Regulates Photoreceptor Differentiation," *Cell* 91 (1997): 531–541.

6. Q. Farjo, A. Jackson, S. Pieke-Dahl, et al., "Human bZIP Transcription Factor Gene NRL: Structure, Genomic Sequence, and Fine Linkage Mapping at 14q11.2 and Negative Mutation Analysis in Patients With Retinal Degeneration," *Genomics* 45 (1997): 395–401.

7. S. G. Jacobson, M. F. Marmor, C. M. Kemp, and R. W. Knighton, "SWS (Blue) Cone Hypersensitivity in a Newly Identified Retinal Degeneration," *Investigative Ophthalmology & Visual Science* 31 (1990): 827–838.

8. A. L. Webber, P. Hodor, C. J. Thut, et al., "Dual Role of Nr2e3 in Photoreceptor Development and Maintenance," *Experimental Eye Research* 87 (2008): 35–48.

9. D. F. Schorderet and P. Escher, "NR2E3 Mutations in Enhanced S-Cone Sensitivity Syndrome (ESCS), Goldmann-Favre Syndrome (GFS), Clumped Pigmentary Retinal Degeneration (CPRD), and Retinitis Pigmentosa (RP)," *Human Mutation* 30 (2009): 1475–1485.

10. M. Toms, N. Ward, and M. Moosajee, "Nuclear Receptor Subfamily 2 Group E Member 3 (NR2E3): Role in Retinal Development and Disease," *Genes* 14 (2023): 1325.

11. F. Coppieters, B. P. Leroy, D. Beysen, et al., "Recurrent Mutation in the First Zinc Finger of the Orphan Nuclear Receptor NR2E3 Causes Autosomal Dominant Retinitis Pigmentosa," *American Journal of Human Genetics* 81 (2007): 147–157.

12. Y. Xu, L. Guan, T. Shen, et al., "Mutations of 60 Known Causative Genes in 157 Families With Retinitis Pigmentosa Based on Exome Sequencing," *Human Genetics* 133 (2014): 1255–1271.

13. D. Sharon, M. A. Sandberg, R. C. Caruso, E. L. Berson, and T. P. Dryja, "Shared Mutations in NR2E3 in Enhanced S-Cone Syndrome, Goldmann-Favre Syndrome, and Many Cases of Clumped Pigmentary Retinal Degeneration," *Archives of Ophthalmology* 121, no. 9 (2003): 1316–1323, https://doi.org/10.1001/archopht.121.9.1316.

14. N. B. Akhmedov, N. I. Piriev, B. Chang, et al., "A Deletion in a Photoreceptor-Specific Nuclear Receptor mRNA Causes Retinal Degeneration in the rd7 Mouse," *Proceedings of the National Academy of Sciences of the United States of America* 97, no. 10 (2000): 5551–5556, https://doi.org/10.1073/pnas.97.10.5551.

15. N. B. Haider, J. K. Naggert, and P. M. Nishina, "Excess Cone Cell Proliferation due to Lack of a Functional NR2E3 Causes Retinal Dysplasia and Degeneration in rd7/rd7 Mice," *Human Molecular Genetics* 10 (2001): 1619–1626.

16. J. C. Chen, A. Rattner, and J. Nathans, "The Rod Photoreceptor-Specific Nuclear Receptor Nr2e3 Represses Transcription of Multiple Cone-Specific Genes," *Journal of Neuroscience* 25 (2005): 118–129.

17. N. B. Haider, P. Demarco, A. M. Nystuen, et al., "The Transcription Factor Nr2e3 Functions in Retinal Progenitors to Suppress Cone Cell Generation," *Visual Neuroscience* 23 (2006): 917–929.

18. S. L. Xie, S. S. Han, Z. Qu, et al., "Knockout of Nr2e3 Prevents Rod Photoreceptor Differentiation and Leads to Selective L−/M-Cone Photoreceptor Degeneration in Zebrafish," *Biochimica et Biophysica Acta—Molecular Basis of Disease* 1865 (2019): 1273–1283.

19. I. Aisa-Marin, M. J. Lopez-Iniesta, S. Milla, et al., "Nr2e3 Functional Domain Ablation by CRISPR-Cas9D10A Identifies a New Isoform and Generates Retinitis Pigmentosa and Enhanced S-Cone Syndrome Models," *Neurobiology of Disease* 146 (2020): 105122.

20. G. Venturini, D. Kokona, B. L. Steiner, et al., "In Vivo Analysis of Onset and Progression of Retinal Degeneration in the Nr2e3(rd7/rd7) Mouse Model of Enhanced S-Cone Sensitivity Syndrome," *Scientific Reports* 11 (2021): 19032.

21. J. C. Corbo and C. L. Cepko, "A Hybrid Photoreceptor Expressing Both Rod and Cone Genes in a Mouse Model of Enhanced S-Cone Syndrome," *PLoS Genetics* 1 (2005): e11.

22. A. H. Milam, L. Rose, A. V. Cideciyan, et al., "The Nuclear Receptor NR2E3 Plays a Role in Human Retinal Photoreceptor Differentiation and Degeneration," *Proceedings of the National Academy of Sciences of the United States of America* 99 (2002): 473–478.

23. F. Hoover, E. A. Seleiro, A. Kielland, P. M. Brickell, and J. C. Glover, "Retinoid X Receptor Gamma Gene Transcripts Are Expressed by a Subset of Early Generated Retinal Cells and Eventually Restricted to Photoreceptors," *Journal of Comparative Neurology* 391 (1998): 204–213.

24. C. Sun, C. Galicia, and D. L. Stenkamp, "Transcripts Within Rod Photoreceptors of the Zebrafish Retina," *BMC Genomics* 19 (2018): 127.

25. N. Jean-Charles, D. F. Buenaventura, and M. M. Emerson, "Identification and Characterization of Early Photoreceptor Cis-Regulatory Elements and Their Relation to Onecut1," *Neural Development* 13 (2018): 26.

26. M. R. Roberts, A. Hendrickson, C. R. McGuire, and T. A. Reh, "Retinoid X Receptor (Gamma) is Necessary to Establish the S-Opsin Gradient in Cone Photoreceptors of the Developing Mouse Retina," *Investigative Ophthalmology & Visual Science* 46 (2005): 2897–2904.

27. A. K. Hennig, G. H. Peng, and S. Chen, "Regulation of Photoreceptor Gene Expression by Crx-Associated Transcription Factor Network," *Brain Research* 1192 (2008): 114–133.

28. Y. Wang, J. Wong, J. L. Duncan, A. Roorda, and W. S. Tuten, "Enhanced S-Cone Syndrome, a Mini-Review," *Advances in Experimental Medicine and Biology* 1415 (2023): 189–194.

29. J. W. Kim, H. J. Yang, A. P. Oel, et al., "Recruitment of Rod Photoreceptors From Short-Wavelength-Sensitive Cones During the Evolution of Nocturnal Vision in Mammals," *Developmental Cell* 37, no. 6 (2016): 520–532.

30. S. Ueno, M. Kondo, K. Miyata, et al., "Physiological Function of S-Cone System Is Not Enhanced in rd7 Mice," *Experimental Eye Research* 81 (2005): 751–758.

31. G. H. Peng, O. Ahmad, F. Ahmad, J. F. Liu, and S. M. Chen, "The Photoreceptor-Specific Nuclear Receptor Nr2e3 Interacts With Crx and Exerts Opposing Effects on the Transcription of Rod Versus Cone Genes," *Human Molecular Genetics* 14 (2005): 747–764.

32. A. J. Mears, M. Kondo, P. K. Swain, et al., "Nrl Is Required for Rod Photoreceptor Development," *Nature Genetics* 29 (2001): 447–452.

33. M. Georgiou, A. G. Robson, K. Fujinami, et al., "Phenotyping and Genotyping Inherited Retinal Diseases: Molecular Genetics, Clinical and Imaging Features, and Therapeutics of Macular Dystrophies, Cone and Cone-Rod Dystrophies, Rod-Cone Dystrophies, Leber Congenital Amaurosis, and Cone Dysfunction Syndromes," *Progress in Retinal and Eye Research* 100 (2004): 101244.

34. S. J. Li, S. Datta, E. Brabbit, et al., "Nr2e3 Is a Genetic Modifier That Rescues Retinal Degeneration and Promotes Homeostasis in Multiple Models of Retinitis Pigmentosa," *Gene Therapy* 28 (2021): 223–241.

35. A. V. Kolesnikov, D. P. Murphy, J. C. Corbo, and V. J. Kefalov, "Germline Knockout of Nr2e3 Protects Photoreceptors in Three Distinct Mouse Models of Retinal Degeneration," *Proceedings of the National Academy of Sciences of the United States of America* 121 (2024): e2316118121.

36. K. P. Weber, C. G. Alvaro, G. M. Baer, et al., "Analysis of *C. Elegans* NR2E Nuclear Receptors Defines Three Conserved Clades and Ligand-Independent Functions," *BMC Evolutionary Biology* 12, no. 1 (2012): 81, https://doi.org/10.1186/1471-2148-12-81.

37. R. Roduit, P. Escher, and D. F. Schorderet, "Mutations in the DNA-Binding Domain of NR2E3 Affect In Vivo Dimerization and Interaction With CRX," *PLoS One* 4 (2009): e7379.

38. J. Fulton, B. Mazumder, J. B. Whitchurch, et al., "Heterodimers of Photoreceptor-Specific Nuclear Receptor (PNR/NR2E3) and Peroxisome Proliferator-Activated Receptor-Gamma (PPARgamma) are Disrupted by Retinal Disease-Associated Mutations," *Cell Death & Disease* 8 (2017): e2677.

39. Y. A. Volonte, V. B. Ayala-Pena, H. Vallese-Maurizi, et al., "Retinoid X Receptor Activation Promotes Photoreceptor Survival and Modulates the Inflammatory Response in a Mouse Model of Retinitis Pigmentosa," *Biochim Biophys Acta Mol Cell Res* 1868, no. 11 (2021): 119098, https://doi.org/10.1016/j.bbamcr.2021.119098.

40. Y. Y. Ding, L. J. Chen, J. Xu, and Q. Liu, "NR2E3 Inhibits the Inflammation and Apoptosis in Diabetic Retinopathy by Regulating the AHR/IL-17A Signaling Pathway," *Naunyn-Schmiedeberg's Archives of Pharmacology* 397 (2024): 9081–9094.

Supporting Information

Additional supporting information can be found online in the Supporting Information section.